

Published online before print January 7, 2008

(Radiology 2008, 10.1148/radiol.2462070536)

© [RSNA](#), 2008**Molecular Imaging***This Article*

- ▶ [Abstract](#) **FRFF**
- ▶ [Figures Only](#)
- ▶ [Appendix E1](#)
- ▶ [Submit a response](#)
- ▶ [Alert me when this article is cited](#)
- ▶ [Alert me when eLetters are posted](#)
- ▶ [Alert me if a correction is posted](#)
- ▶ [Citation Map](#)

Services

- ▶ [Email this article to a friend](#)
- ▶ [Similar articles in this journal](#)
- ▶ [Similar articles in PubMed](#)
- ▶ [Alert me to new issues of the journal](#)
- ▶ [Download to citation manager](#)
- ▶ [© Get Permissions](#)

Google Scholar

- ▶ [Articles by Willmann, J. K.](#)
- ▶ [Articles by Gambhir, S. S.](#)

PubMed

- ▶ [PubMed Citation](#)
- ▶ [Articles by Willmann, J. K.](#)
- ▶ [Articles by Gambhir, S. S.](#)

US Imaging of Tumor Angiogenesis with Microbubbles Targeted to Vascular Endothelial Growth Factor Receptor Type 2 in Mice¹

Jürgen K. Willmann, MD, Ramasamy Paulmurugan, PhD, Kai Chen, PhD, Olivier Gheysens, MD, Martin Rodriguez-Porcel, MD, Amelie M. Lutz, MD, Ian Y. Chen, MSE, Xiaoyuan Chen, PhD, and Sanjiv S. Gambhir, MD, PhD

1

From the Molecular Imaging Program at Stanford, Department of Radiology and Bio-X Program (J.K.W., R.P., K.C., O.G., M.R., A.M.L., I.Y.C., X.C., S.S.G.), and Department of Bioengineering (I.Y.C., S.S.G.), Stanford University School of Medicine, the James H. Clark Center, 318 Campus Dr, East Wing, 1st Floor, Stanford, CA 94305-5427. Received January 15, 2007; revision requested May 23; revision received June 9; final version accepted August 1. Supported by the Swiss Foundation of Medical-Biological Grants (J.K.W.); Novartis Research Foundation (J.K.W.); Swiss Society of Radiology (J.K.W.); in part by grants NCI SAIRP (S.S.G.), NHLBI 1 R01 HL078632 (S.S.G.), NCI ICMIC CA114747 P50 (S.S.G.); and the Canary Foundation. **Address correspondence to** S.S.G. (e-mail: sgambhir@stanford.edu).

**ABSTRACT**

Purpose: To prospectively evaluate contrast material-enhanced ultrasonography (US) with microbubbles targeted to vascular

- ▲ [TOP](#)
- [ABSTRACT](#)
- ▼ [INTRODUCTION](#)

endothelial growth factor receptor type 2 (VEGFR2) for imaging tumor angiogenesis in two murine tumor models.

Materials and Methods: Animal protocols were approved by the Institutional Administrative Panel on Laboratory Animal Care. A US contrast agent, consisting of encapsulated gaseous microbubbles, was developed specifically to bind to VEGFR2 (by using anti-VEGFR2 antibodies and biotin-streptavidin interaction) which is up-regulated on endothelial cells of tumor blood vessels. VEGFR2-targeted microbubbles (MB_V), control microbubbles (MB_C), and nonlabeled microbubbles (MB_N) were tested for binding specificity on cells expressing VEGFR2 (mouse angiosarcoma SVR cells) and control cells (mouse skeletal myoblast C2C12 cells). Expression of mouse VEGFR2 in culture cells was tested with immunocytochemical and Western blot analysis. Contrast-enhanced US imaging with MB_V and MB_C was performed in 28 tumor-bearing nude mice (mouse angiosarcoma, $n = 18$; rat malignant glioma, $n = 10$). Differences were calculated by using analysis of variance.

Results: In cell culture, adherence of MB_V on SVR cells (2.1 microbubbles per SVR cell) was significantly higher than adherence of control microbubbles (0.01–0.10 microbubble per SVR cell; $P < .001$) and significantly more MB_V attached to SVR cells than to C2C12 cells (0.15 microbubble per C2C12 cell; $P < .001$). In vivo, contrast-enhanced US imaging showed significantly higher average video intensity when using MB_V compared with MB_C for angiosarcoma and malignant glioma tumors ($P < .001$). Results of immunohistochemical analysis confirmed VEGFR2 expression on vascular endothelial cells of both tumor types.

Conclusion: US imaging with contrast microbubbles targeted to VEGFR2 allows noninvasive visualization of VEGFR2 expression in tumor vessels in mice.

© RSNA, 2008

Supplemental material: <http://radiology.rsna.org/cgi/content/full/2462070536/DC1/>

► INTRODUCTION

Angiogenesis, the recruitment of new blood vessels, is promoted early with cancer cells in tumorigenesis and is a critical determinant of tumor growth, invasion, and metastatic potential (1). Several specific endothelial molecular markers of angiogenesis, including vascular endothelial growth factor (VEGF) receptor type 2 (VEGFR2), are overexpressed on tumor vascular endothelial cells. VEGFR2 is one of the major regulators of angiogenesis, and activation of the VEGF/VEGFR2 axis triggers multiple signaling networks that result in endothelial cell survival, mitogenesis, migration, differentiation, and vascular permeability (2).

Overexpression of VEGF and/or VEGFR2 has been associated with tumor progression and poor prognosis in several tumors, including colorectal, gastric, and pancreatic carcinomas; angiosarcomas; breast, prostate, and lung cancers; malignant gliomas; and melanoma (2). Bevacizumab (Avastin Genentech, San Francisco, Calif), the first angiogenesis inhibitor approved by the U.S. Food and Drug Administration, targets the VEGF/VEGFR2 axis, and was the first used to demonstrate prolonged survival in patients with advanced cancer (3). Thus, imaging strategies that can directly depict specific molecular markers of angiogenesis, such as VEGFR2, may be

- ▼ [MATERIALS AND METHODS](#)
- ▼ [RESULTS](#)
- ▼ [DISCUSSION](#)
- ▼ [ADVANCE IN KNOWLEDGE](#)
- ▼ [IMPLICATION FOR PATIENT CARE](#)
- ▼ [References](#)

- ▲ [TOP](#)
- ▲ [ABSTRACT](#)
- [INTRODUCTION](#)
- ▼ [MATERIALS AND METHODS](#)
- ▼ [RESULTS](#)
- ▼ [DISCUSSION](#)
- ▼ [ADVANCE IN KNOWLEDGE](#)
- ▼ [IMPLICATION FOR PATIENT CARE](#)
- ▼ [References](#)

particularly advantageous for tracking antiangiogenic tumoricidal treatments and development of cancer therapies.

Ultrasonography (US) is a widely used imaging modality which offers high spatial resolution, allows real-time imaging, and combines the advantages of noninvasiveness with the lack of ionizing radiation. US contrast agents are gas-filled, echogenic microbubbles that remain exclusively in the vascular compartment (4). By using site labeling to target microbubbles to specific molecular markers, it has recently been shown that contrast material-enhanced US allows detection of specific intravascular molecular markers of tumor angiogenesis (5–7). To our knowledge, no study has systematically addressed the potential of targeted US imaging for a spatial and quantitative assessment of tumor angiogenesis in cell culture and in vivo by using microbubbles targeted to VEGFR2 (MB_V).

Thus, the purpose of our study was to prospectively evaluate contrast-enhanced US with MB_V for imaging tumor angiogenesis in two murine tumor models.

▶ MATERIALS AND METHODS

Visualsonics (Toronto, Canada) provided the microbubbles used in this study. All authors who were not consultants of Visualsonics had control of inclusion of any data and information that might present a conflict of interest for those authors who were consultants of Visualsonics.

Cell Culture Experiments

Cell lines.—Mouse angiosarcoma SVR cells, mouse skeletal myoblast (C2C12) cells, and rat malignant glioma (C6) cells (all purchased from American Tissue Type Collection, Manassas, Va) were grown in Dulbecco's modified Eagle's medium with a high concentration of glucose (4.5 g/L) and L-glutamine (Invitrogen, Carlsbad, Calif), and supplemented with 10% fetal bovine serum and penicillin (100 U/mL) and streptomycin (100 µg/mL). Cells were harvested by using trypsinization at 80%–90% confluence.

Targeted microbubbles.—Lipid-shelled microbubbles (8.4×10^8) containing perfluorocarbon contrast agents (MicroMarker; Bracco Research, Geneva, Switzerland) were resuspended in 1000 µL sterile saline (0.9% sodium chloride), according to the manufacturer's instructions. These microbubbles have a mean diameter of 1.5 µm (range, 1–2 µm) as assessed by using a cell counter and sizer (Multisizer III Coulter Counter; Beckman Coulter, Fullerton, Calif) and contain approximately 7600 molecules streptavidin per square micrometer. MB_V were synthesized by coupling the rat anti-mouse VEGFR2 monoclonal antibody (Avas 12a1; eBioscience, San Diego, Calif) by using biotin-streptavidin interaction.

This coupling strategy resulted in approximately 6000 ligands per square micrometer of surface area, as determined by incubating iodine 125-labeled biotinylated rat anti-mouse VEGFR2 monoclonal antibody with the streptavidin-containing microbubbles. Control microbubbles (MB_C) conjugated with biotinylated isotype-matched control rat immunoglobulin G2 antibody (eBioscience) and nontargeted microbubbles (MB_N) without conjugated antibody were also prepared. Excess unbound antibody was removed by washing in phosphate-buffered saline (PBS).

Immunocytochemical analysis.—SVR and C2C12 cells (4×10^5) were grown on different coverslips for 24

- ▲ [TOP](#)
- ▲ [ABSTRACT](#)
- ▲ [INTRODUCTION](#)
- [MATERIALS AND METHODS](#)
- ▼ [RESULTS](#)
- ▼ [DISCUSSION](#)
- ▼ [ADVANCE IN KNOWLEDGE](#)
- ▼ [IMPLICATION FOR PATIENT CARE](#)
- ▼ [References](#)

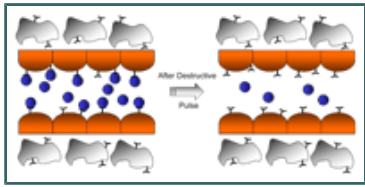
hours. Cells were fixed in 4% formaldehyde for 1 minute, washed in PBS, and blocked in 2% bovine serum albumin for 1 hour. Cells were then incubated with a rabbit anti-mouse VEGFR2 antibody in a 1:2000 ratio (Upstate, Lake Placid, NY) for 30 minutes at 37°C, washed in PBS, and incubated with fluorescein isothiocyanate-labeled goat anti-rabbit secondary antibody in a 1:200 ratio (Chemicon, Temecula, Calif) for 30 minutes at 37°C. Separate cells were also incubated with the fluorescent secondary antibody or with the primary antibody alone to exclude nonspecific cellular interactions. Coverslips were mounted on glass microscope slides by using an adhesive (Cytoseal XYL; Microm International, Walldorf, Germany). Fluorescent microscopy (excitation filter, 365 nm) of washed cells was performed with a microscope (Axiovert 25; Carl Zeiss, Thornwood, NY) and a camera (AxioCam, Bernried, Germany). Studies were performed in triplicate.

Western blotting.—SVR and C2C12 cells were lysed by using sonication. Twenty micrograms of protein were separated by a 4%–12% bis-tris gradient gel (NuPAGE, Invitrogen). The protein was transferred to a nitrocellulose membrane by using a semidry electroblot apparatus (Hoefer TE 70; Amersham Bioscience, Piscataway, NJ) and blocked with 5% nonfat milk powder in tris(hydroxymethyl)aminomethanebuffered saline with 0.05% Tween 20 (Sigma, St Louis, Mo) for 1 hour. The membrane was incubated with a rabbit anti-mouse VEGFR2 primary antibody in a 1:2000 ratio (Upstate) for 12 hours at 4°C. The washed membrane was then incubated with a horseradish peroxidase-conjugated anti-rabbit secondary antibody in a 1:5000 ratio (Promega, Madison, Wis) for 1 hour at room temperature and washed twice with tris(hydroxymethyl)aminomethane-buffered saline with Tween 20. The enhanced chemiluminescence detection kit (GE Healthcare, Piscataway, NJ) was used for exposure to x-ray film. As an internal loading control, the same membrane was washed and incubated with anti- α -tubulin antibody. Studies were performed in triplicate.

Cell attachment studies.—SVR and C2C12 cells (1×10^5) were grown for 24 hours on different coverslips. Coverslips were incubated in 3 mL PBS containing 5×10^7 MB_V, 5×10^7 MB_C, or 5×10^7 MB_N. The number of microbubbles was obtained by using the cell counter and sizer. Owing to the buoyancy of the microbubbles, the coverslips were inverted to maximize exposure of the cells to the microbubbles. After a 4-minute static exposure, the coverslips were washed in PBS to remove unbound microbubbles. Studies were also performed 30 minutes after antibody blockage (30 μ g/mL; eBioscience) of rat anti-mouse VEGFR2. All studies were performed in triplicate.

The mean number of cell-attached microbubbles in five randomly selected optical fields was determined by using microscopy (original magnification, $\times 400$) for each coverslip by one reader (reader 1, R.P., with 1 year experience) who was blinded to the types of microbubbles and cells. Microbubbles can be directly visualized as small, rounded structures and the number of attached microbubbles and the number of cells can be counted to obtain the number of attached microbubbles per cell (8).

SVR cells (which express VEGFR2, see below) and C2C12 cells (which do not express VEGFR2 as a negative control cell line, see below) were used only for cell culture experiments to test attachment of different types of microbubbles to VEGFR2. SVR and C6 cells were also injected into nude mice to create a fast-growing tumor model known to demonstrate tumor angiogenesis (9–12). Since the microbubbles stay exclusively within the vascular compartment owing to their size (4), in our study, only VEGFR2 on endothelial cells of tumor vessels were targeted in vivo, not VEGFR2 on SVR tumor cells (Fig 1).



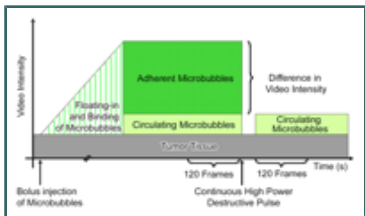
View larger version (27K):

[\[in this window\]](#)

[\[in a new window\]](#)

[\[Download PPT slide\]](#)

Figure 1a: Targeted US of tumor angiogenesis in angiosarcoma tumor. **(a)** Tumor consists of tumor cells (gray) and tumor vessels with neoplastic endothelial cells (orange). In angiosarcoma tumors (obtained with injection of SVR cells), tumor cells and neoplastic endothelial cells express VEGFR2. Owing to relatively large microbubble (blue) size (several micrometers), they remain exclusively in vascular compartment after intravenous administration and adhere to neoplastic endothelial cells of tumor vessels but not to tumor cells. Note additional freely circulating microbubbles. After high-power destructive pulse, adherent microbubbles are destroyed and freely circulating microbubbles replenish from outside imaging plane after several seconds. **(b)** Summary of video intensity components at contrast-enhanced US before and after high-power destructive pulse. After intravenous injection, microbubbles float in tumor vessels and bind to VEGFR2. Four minutes later, video intensity has three components: video intensity from tumor tissue, video intensity from microbubbles not attached to receptors (circulating microbubbles), and video intensity from microbubbles attached to receptors on neoplastic endothelial cells. After digital subtraction of 120 predestruction frames from 120 postdestruction frames (acquired 9 seconds post destruction), resulting video intensity is attributable to adherent microbubbles.



View larger version (24K):

[\[in this window\]](#)

[\[in a new window\]](#)

[\[Download PPT slide\]](#)

Figure 1b: Targeted US of tumor angiogenesis in angiosarcoma tumor. **(a)** Tumor consists of tumor cells (gray) and tumor vessels with neoplastic endothelial cells (orange). In angiosarcoma tumors (obtained with injection of SVR cells), tumor cells and neoplastic endothelial cells express VEGFR2. Owing to relatively large microbubble (blue) size (several micrometers), they remain exclusively in vascular compartment after intravenous administration and adhere to neoplastic endothelial cells of tumor vessels but not to tumor cells. Note additional freely circulating microbubbles. After high-power destructive pulse, adherent microbubbles are destroyed and freely circulating microbubbles replenish from outside imaging plane after several seconds. **(b)** Summary of video intensity components at contrast-enhanced US before and after high-power destructive pulse. After intravenous injection, microbubbles float in tumor vessels and bind to VEGFR2. Four minutes later, video intensity has three components: video intensity from tumor tissue, video intensity from microbubbles not attached to receptors (circulating microbubbles), and video intensity from microbubbles attached to receptors on neoplastic endothelial cells. After digital subtraction of 120 predestruction frames from 120 postdestruction frames (acquired 9 seconds post destruction), resulting video intensity is attributable to adherent microbubbles.

Small-Animal Imaging Experiments

Animal protocols were approved by the Institutional Administrative Panel on Laboratory Animal Care. Tumors were established by one author (J.K.W., with 1 year experience) in 28 female 6–8-week-old nude mice (Charles River Laboratories, Wilmington, Mass) in random order by subcutaneous injection of a suspension of either 3×10^6 SVR cells ($n = 18$) or 3×10^6 C6 cells ($n = 10$) in $50 \mu\text{L}$ PBS in the right flank region. The mice were anesthetized with 2% isoflurane in oxygen at 2 L/min during the injections. Tumors (mouse angiosarcoma and rat malignant glioma tumors) were allowed to grow for 7–21 days (mean maximum diameter at US, 5 mm; range,

3–9 mm). Five non-tumor-bearing mice were used as a quasi-tumor angiogenesis-negative model (see below).

Targeted Contrast-enhanced US Imaging

Animal preparation, US settings, and B-mode imaging.—US imaging was performed by one author (reader 2, J.K.W., with 8 years experience) by using a dedicated small-animal high-resolution imaging unit (Vevo 770; VisualSonics, Toronto, Canada) and a 40-MHz high-frequency linear transducer (lateral resolution, 100 μm ; transverse resolution, 40 μm ; focal length, 6 mm; mechanical index, 0.14; transmit power, 50%; dynamic range, 52 dB). All imaging was performed in fundamental brightness mode (B mode). Reader 2 was aware of the tumor type and the type of microbubbles administered in the mice. Throughout the imaging session, mice were kept anesthetized with 2% isoflurane in oxygen at 2 L/min on a heated stage with constant monitoring of their body temperature by using a rectal temperature probe. Prewarmed US gel was used as a coupling agent on the skin of the mice. Real-time imaging was performed with a frame rate of 20 Hz (corresponding to a temporal resolution of 50 msec). Two-dimensional B-mode image planes were acquired with optimization of the gain and the time gain compensation settings, which were kept constant throughout the experiment. The acoustic focus was placed at the center of the tumor at the level of the largest transverse cross section and maintained throughout each experiment.

Contrast-enhanced US image protocol.—The goal of the US image protocol was to differentiate between the acoustic signal owing to adherent MB_V and the signal from MB_V still freely circulating in the bloodstream. For this purpose, we used previously described principles of US-induced microbubble destruction and replenishment (Appendix E1, <http://radiology.rsnajnl.org/cgi/content/full/2462070536/DC1>; Fig 1) (13,14). After intravenous injection of 5×10^7 MB_V (60 μL) in the tail vein of the mice (injection time, 3 seconds), imaging was paused for 4 minutes to allow retention of the microbubbles. One hundred twenty frames were then captured over a 6-second period to obtain a signal from the tumor tissue as well as from adherent and freely circulating microbubbles (Fig 1). A continuous 10-MHz high-power destructive pulse (mechanical index, ~ 0.235 ; average power, ~ 0.0676 W/cm²) was then applied for 3 seconds, which destroyed the microbubbles within the beam elevation. Nine seconds after destruction (to allow freely circulating microbubbles to replenish in tumor vessels within the beam elevation), 120 frames were acquired with the same US settings as before the pulse, containing signal from the tumor tissue and from freely circulating microbubbles (Fig 1). These signals were averaged and digitally subtracted from the initial predestruction frames to derive the signal attributable on adherent MB_V only (Fig 1).

Reproducibility of the image protocol of targeted contrast-enhanced US imaging was tested in five angiosarcoma tumor-bearing mice. Mice were scanned according to the protocol mentioned above. After 24 hours, scanning with the same US settings as the first imaging session was repeated with a second injection of microbubbles and with the transducer as close as possible to the US imaging plane of the first imaging session by marking the position of the transducer on the skin of the mice at the first imaging session.

Testing of VEGFR2 specificity of US signal.—To test the specificity of the signal coming from adherent MB_V we also injected 5×10^7 MB_C and 5×10^7 MB_N in the same animal, during the same imaging session, for all mice. The different types of microbubbles were administered in random order to minimize any bias. To allow clearance of microbubbles from the preceding imaging sessions, a 30-minute delay was used between each imaging session. This delay between microbubble injections was chosen on the basis of other results (7); our experience was that most of the microbubbles cleared from the vasculature in 30 minutes after intravenous injection.

To further test the specificity of the signal coming from MB_V, in vivo blocking studies were performed in a

subset of five angiosarcoma tumor-bearing mice. Animals were first scanned by using the imaging protocol described above. Subsequently, 125 μg of a rat anti-mouse VEGFR2 monoclonal antibody (250 μL Avas) was injected in the tail vein. After 30 minutes, to allow distribution of the antibodies in the tissue, targeted US imaging by using MBV was repeated.

Finally, as a quasi-tumor angiogenesis-negative model, targeted US imaging of normal skeletal muscle (hind limb adductor muscles) of five additional nontumor-bearing nude mice was performed to assess magnitude of persistent contrast enhancement of nonneoplastic and nonangiogenesis microvasculature after injection of MBV. For this purpose, the same transducer was placed on the hind limb adductor muscle and the skeletal muscle was scanned by using the imaging protocol described above.

Image Analysis

Images were recorded digitally and analyzed offline by using commercially available high-resolution micro-US imaging software (Vevo 770; Visualsonics). Image analysis was performed in random order by one radiologist (reader 3, A.M.L., with 7 years experience) who was blinded to the types of administered microbubbles. Average image brightness (video intensity, which corresponds to the 8-bit log-compressed gray scale) was measured in regions of interest encompassing the whole tumor in the imaging plane (mean area, 20 mm^2 ; range, 7–49 mm^2). The difference in video intensity from subtraction of the pre- and postdestruction image frames (see above) was automatically displayed by the software as a colored (green) overlay on the gray-scale images. For assessment of contrast enhancement in hind limb muscles, a region of interest was set to encompass the adductor muscle (mean area, 10 mm^2 ; range, 5–14 mm^2). To measure the signal from specific adhesion of the microbubbles to mouse VEGFR2 the mean video intensity difference (VI_T) for MBV injections minus the VI_T for MBC injections, in the same mouse was calculated (7).

Tumor Immunohistochemistry

After US imaging, the animals were euthanized and the tumors were harvested. Frozen tissue slices (5- μm thickness) of the tumors were fixed with cold acetone for 10 minutes and dried in air for 30 minutes. The slices were rinsed with PBS for 2 minutes and blocked with 10% donkey serum for 30 minutes at room temperature. The slices were then incubated with rat anti-mouse VEGFR2 antibody (DC101; ImClone Systems, New York, NY) overnight at 4°C and visualized by using Cy3-conjugated donkey anti-rat secondary antibody in a 1:200 ratio (Jackson ImmunoResearch Laboratories, West Grove, Pa). Consecutive slices from each sample were used for CD31 staining (a marker for endothelial cells) to compare VEGFR2 expression with tumor vessels. For this purpose, the slices were incubated with rat anti-mouse CD31 antibody in a 1:100 ratio (BD Biosciences, San Jose, Calif) at room temperature for 1 hour and visualized with fluorescein isothiocyanate-conjugated donkey anti-rat antibody in a 1:200 ratio (Jackson ImmunoResearch Laboratories). To identify the nuclei, CD31-stained slices were counterstained with 4',6-diamidino-2-phenylindole (DAPI; Sigma-Aldrich, St Louis, Mo). Representative pictures were taken of randomly chosen fields of view by one author (K.C., with 4 years experience) by using a microscope and a camera.

Statistical Analysis

Data are reported as mean \pm standard deviation. In cell culture experiments, a two-way fixed-effects analysis of variance was performed on the mean number of microbubbles attached to the cells, by using the three different types of microbubbles and the two different cell lines as factors. The coefficient of variation, defined as (standard deviation/mean)·100, was calculated to describe reproducibility of the image protocol of targeted contrast-enhanced US imaging. In addition, a one-way random-effect analysis of variance was performed to assess the between-animal and within-animal variance components (test-retest reliability).

To assess the effect of microbubble type in in vivo experiments, two repeated-measures analyses of variance were performed. First, a two-way analysis of variance was performed which included all animals and used the three types of microbubbles and the two tumor types as factors with different types of microbubbles used as the repeated measure. Second, a one-way analysis of variance was performed in a subset of five mice that underwent an in vivo VEGFR2-blocking experiment. Finally, a one-way between-subject analysis of variance was performed to compare video intensities by using VEGFR2-targeted and isotype-control immunoglobulin G2-labeled microbubbles between the tumor groups and an additional group of five mice with nonneoplastic/nonangiogenesis microvasculature in hind limb muscle. Greenhouse-Geisser adjustments were made to *P* values to correct for lack of sphericity in the residuals.

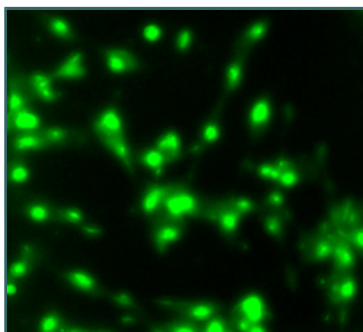
All statistical analyses were performed with software (Stata, version 9.2; Stata, College Station, Tex). A *P* value of less than .05 was considered to indicate a significant difference.

RESULTS

Cell Culture Experiments

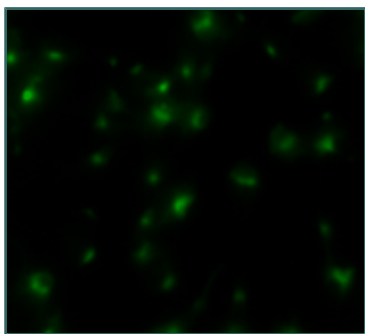
Immunocytochemical staining for mouse VEGFR2 expression was positive for SVR cells and negative for C2C12 cells (Fig 2). Presence of mouse VEGFR2 in SVR cells was further confirmed by using Western blotting (Fig 2). There were highly significant differences among each microbubble type ($P < .001$) and cell line ($P < .001$), as well as an interaction between them ($P < .001$), owing to the higher VEGFR2 binding rate in SVR versus C2C12 cells. After a static exposure of the SVR and C2C12 cells to MB_V, adherence of MB_V was significantly higher to SVR cells compared with negative control C2C12 cells ($P < .001$) (Fig 3; Table 1). MB_C and MB_N adhered minimally to SVR cells. Adherence of MB_V to SVR cells was 21 times higher compared with MB_C ($P < .001$). There was almost no binding of MB_N to SVR and C2C12 cells. MB_V attachment to SVR cells was significantly reduced after preincubation with anti-mouse VEGFR2 antibodies ($P < .001$) (Table 1). During the experiments, no microbubble internalization in the cells was observed.

- ▲ [TOP](#)
- ▲ [ABSTRACT](#)
- ▲ [INTRODUCTION](#)
- ▲ [MATERIALS AND METHODS](#)
- [RESULTS](#)
- ▼ [DISCUSSION](#)
- ▼ [ADVANCE IN KNOWLEDGE](#)
- ▼ [IMPLICATION FOR PATIENT CARE](#)
- ▼ [References](#)



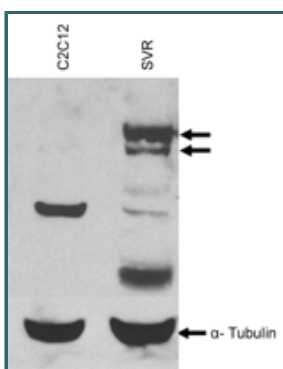
View larger version (146K):
[\[in this window\]](#)
[\[in a new window\]](#)
[\[Download PPT slide\]](#)

Figure 2a: Immunofluorescence staining of (a) SVR cells (positive) and (b) C2C12 cells (negative) for VEGFR2. Note slight fluorescence in C2C12 cells owing to autofluorescence, of cell nucleus in particular. Cells were stained with rabbit anti-mouse VEGFR2 primary antibody and fluorescein isothiocyanate-labeled goat anti-rabbit secondary antibody. (c) Western blot analysis of VEGFR2 expression in SVR and C2C12 cells. Twenty micrograms of protein were assessed for VEGFR2 expression in SVR and C2C12 cells by using rabbit anti-mouse VEGFR2 primary antibody (recognizing VEGFR2 [200–230 kDa] and immature protein form [180–200 kDa]; arrows), HRP-conjugated anti-rabbit secondary antibody, and chemiluminescence detection system. α -Tubulin expression was used as loading control. VEGFR2 was detected in SVR (arrows) but not in C2C12 cell lysates.



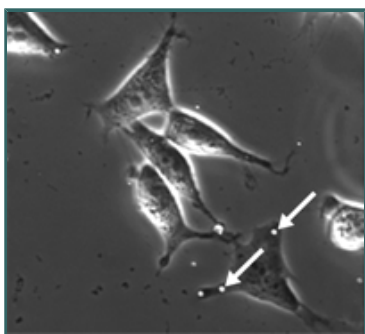
View larger version (53K):
[\[in this window\]](#)
[\[in a new window\]](#)
[\[Download PPT slide\]](#)

Figure 2b: Immunofluorescence staining of (a) SVR cells (positive) and (b) C2C12 cells (negative) for VEGFR2. Note slight fluorescence in C2C12 cells owing to autofluorescence, of cell nucleus in particular. Cells were stained with rabbit anti-mouse VEGFR2 primary antibody and fluorescein isothiocyanate–labeled goat anti-rabbit secondary antibody. (c) Western blot analysis of VEGFR2 expression in SVR and C2C12 cells. Twenty micrograms of protein were assessed for VEGFR2 expression in SVR and C2C12 cells by using rabbit anti-mouse VEGFR2 primary antibody (recognizing VEGFR2 [200–230 kDa] and immature protein form [180–200 kDa]; arrows), HRP-conjugated anti-rabbit secondary antibody, and chemiluminescence detection system. α -Tubulin expression was used as loading control. VEGFR2 was detected in SVR (arrows) but not in C2C12 cell lysates.



View larger version (52K):
[\[in this window\]](#)
[\[in a new window\]](#)
[\[Download PPT slide\]](#)

Figure 2c: Immunofluorescence staining of (a) SVR cells (positive) and (b) C2C12 cells (negative) for VEGFR2. Note slight fluorescence in C2C12 cells owing to autofluorescence, of cell nucleus in particular. Cells were stained with rabbit anti-mouse VEGFR2 primary antibody and fluorescein isothiocyanate–labeled goat anti-rabbit secondary antibody. (c) Western blot analysis of VEGFR2 expression in SVR and C2C12 cells. Twenty micrograms of protein were assessed for VEGFR2 expression in SVR and C2C12 cells by using rabbit anti-mouse VEGFR2 primary antibody (recognizing VEGFR2 [200–230 kDa] and immature protein form [180–200 kDa]; arrows), HRP-conjugated anti-rabbit secondary antibody, and chemiluminescence detection system. α -Tubulin expression was used as loading control. VEGFR2 was detected in SVR (arrows) but not in C2C12 cell lysates.



View larger version (105K):
[\[in this window\]](#)
[\[in a new window\]](#)
[\[Download PPT slide\]](#)

Figure 3a: Bright-field micrographs show SVR cells expressing (a–c) VEGFR2 and (d–f) C2C12 cells without VEGFR2 expression after exposure to MB_V (a and d), MB_C (b and e), and MB_N (c and f). MB_V preferentially attached to SVR cells, MB_C rarely attached to either cell type. Microbubbles are small rounded structures (arrows). (Original magnification, x400.)

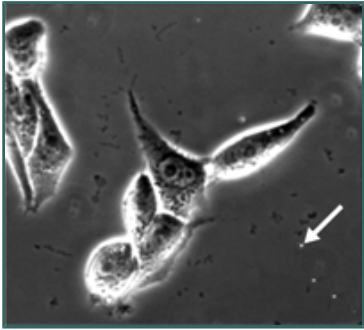


Figure 3b: Bright-field micrographs show SVR cells expressing (a–c) VEGFR2 and (d–f) C2C12 cells without VEGFR2 expression after exposure to MB_V (a and d), MB_C (b and e), and MB_N (c and f). MB_V preferentially attached to SVR cells', MB_C rarely attached to either cell type. Microbubbles are small rounded structures (arrows). (Original magnification, x400.)

View larger version (126K):

[\[in this window\]](#)

[\[in a new window\]](#)

[\[Download PPT slide\]](#)

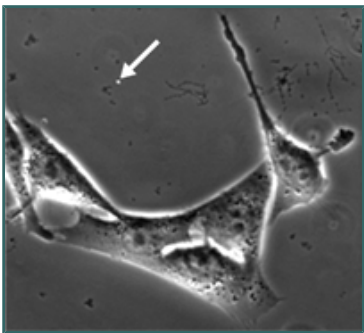


Figure 3c: Bright-field micrographs show SVR cells expressing (a–c) VEGFR2 and (d–f) C2C12 cells without VEGFR2 expression after exposure to MB_V (a and d), MB_C (b and e), and MB_N (c and f). MB_V preferentially attached to SVR cells', MB_C rarely attached to either cell type. Microbubbles are small rounded structures (arrows). (Original magnification, x400.)

View larger version (126K):

[\[in this window\]](#)

[\[in a new window\]](#)

[\[Download PPT slide\]](#)

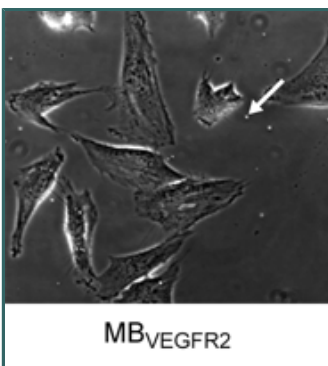


Figure 3d: Bright-field micrographs show SVR cells expressing (a–c) VEGFR2 and (d–f) C2C12 cells without VEGFR2 expression after exposure to MB_V (a and d), MB_C (b and e), and MB_N (c and f). MB_V preferentially attached to SVR cells', MB_C rarely attached to either cell type. Microbubbles are small rounded structures (arrows). (Original magnification, x400.)

View larger version (111K):

[\[in this window\]](#)

[\[in a new window\]](#)

[\[Download PPT slide\]](#)

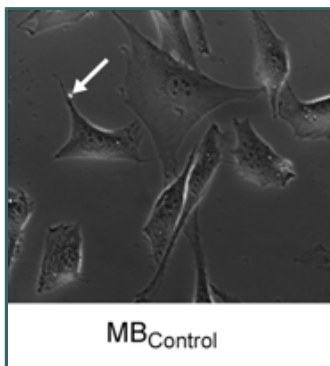


Figure 3e: Bright-field micrographs show SVR cells expressing (a–c) VEGFR2 and (d–f) C2C12 cells without VEGFR2 expression after exposure to MB_V (a and d), MB_C (b and e), and MB_N (c and f). MB_V preferentially attached to SVR cells', MB_C rarely attached to either cell type. Microbubbles are small rounded structures (arrows). (Original magnification, x400.)

View larger version (86K):

[\[in this window\]](#)

[\[in a new window\]](#)

[\[Download PPT slide\]](#)

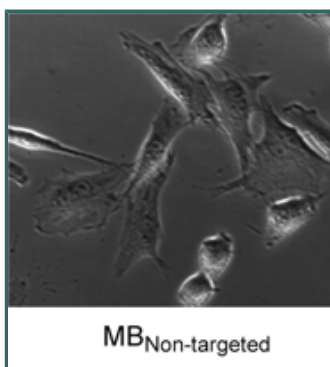


Figure 3f: Bright-field micrographs show SVR cells expressing (a–c) VEGFR2 and (d–f) C2C12 cells without VEGFR2 expression after exposure to MB_V (a and d), MB_C (b and e), and MB_N (c and f). MB_V preferentially attached to SVR cells', MB_C rarely attached to either cell type. Microbubbles are small rounded structures (arrows). (Original magnification, x400.)

View larger version (95K):

[\[in this window\]](#)

[\[in a new window\]](#)

[\[Download PPT slide\]](#)

View this table: [Table 1. Attachment of Different Types of Microbubbles to SVR and C2C12 Cells in Cell Culture Experiments](#)

[\[in this window\]](#)

[\[in a new window\]](#)

Small-Animal Imaging Experiments

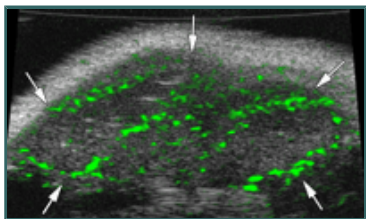
Regarding the reproducibility of targeted contrast-enhanced US imaging in five angiosarcoma tumor-bearing mice, which were scanned on 2 consecutive days ([Table 2](#)), the mean coefficient of variation of VI_T between the two imaging sessions was $11.1\% \pm 3.8$ and the mean difference of the VI_T was 6.4 intensity units ± 4.3 (intraclass correlation of 0.88; 95% confidence interval: 0.69, 0.99). Tumor size (mean maximum diameter, 3.5 mm; range 3–4.5 mm), as assessed by using US imaging, was not significantly different within 24 hours for each animal ($P < .157$, paired Wilcoxon test).

View this table: [Table 2. VI_T, Differences in Video Intensity between Scans, and Coefficients of](#)

[\[in this window\]](#) **Variation in Five Angiosarcoma Tumor-bearing Mice as Determined from**
[\[in a new window\]](#) **Repeat Targeted Contrast-enhanced US**

Regarding the average quantitative video intensity data for angiosarcoma ($n = 18$) and malignant glioma ($n = 10$) tumors as obtained with contrast-enhanced US imaging in living mice ([Table 3](#)), the repeated-measures analysis of variance for all animals indicated a highly significant effect for microbubble type ($P < .001$), a marginal effect for tumor type ($P < .040$), and no significant interaction between them ($P < .083$). For angiosarcoma and malignant glioma tumors, the average video intensity was significantly higher when using MB_V versus MB_C ($P < .001$) ([Fig 4](#)). There was only a small signal when using MB_N. VI_T , defined as the mean video intensity difference for MB_C injections subtracted from the mean video intensity difference for MB_V injections, was 34.4 intensity units for angiosarcoma tumors and 28.4 intensity units for malignant glioma tumors. Both were significantly higher ($P < .001$) than for nonneoplastic/nonangiogenesis vasculature in normal skeletal muscle tissue which was used as a negative control (two intensity units, $P < .001$).

View this table: [Table 3. Quantitative Video Intensity Difference Data for Contrast-enhanced US Images of Tumor Vessels Following Intravenous Microbubble Administration](#)
[\[in this window\]](#)
[\[in a new window\]](#)



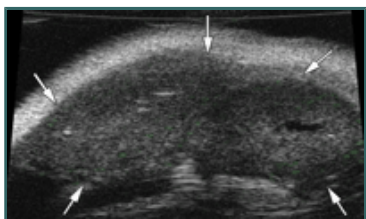
View larger version (108K):

[\[in this window\]](#)

[\[in a new window\]](#)

[\[Download PPT slide\]](#)

Figure 4a: Transverse color-coded US images of subcutaneous 9-mm malignant glioma tumor (arrows) in same nude mouse. Images obtained 4 minutes after intravenous administration of (a) MB_V, (b) MB_C, or (c) MB_N (see Results). Differences in video intensity from subtraction of pre- and postdestruction images (green) on gray scale images were higher with MB_V than with MB_C. No signal was detected after MB_N application.



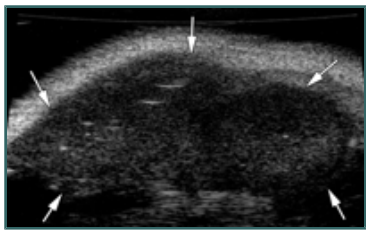
View larger version (111K):

[\[in this window\]](#)

[\[in a new window\]](#)

[\[Download PPT slide\]](#)

Figure 4b: Transverse color-coded US images of subcutaneous 9-mm malignant glioma tumor (arrows) in same nude mouse. Images obtained 4 minutes after intravenous administration of (a) MB_V, (b) MB_C, or (c) MB_N (see Results). Differences in video intensity from subtraction of pre- and postdestruction images (green) on gray scale images were higher with MB_V than with MB_C. No signal was detected after MB_N application.



View larger version (94K):

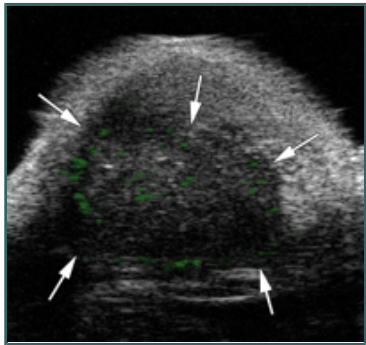
[\[in this window\]](#)

[\[in a new window\]](#)

[\[Download PPT slide\]](#)

Figure 4c: Transverse color-coded US images of subcutaneous 9-mm malignant glioma tumor (arrows) in same nude mouse. Images obtained 4 minutes after intravenous administration of (a) MB_V, (b) MB_C, or (c) MB_N (see Results). Differences in video intensity from subtraction of pre- and postdestruction images (green) on gray scale images were higher with MB_V than with MB_C. No signal was detected after MB_N application.

In the subset of five (28%) of 18 angiosarcoma tumor-bearing mice, which were also scanned 30 minutes after administration of anti-mouse VEGFR2 antibodies, VI_T dropped by 63.5% from 34.8 to 12.7 intensity units ($P < .001$) (Fig 5).



View larger version (153K):

[\[in this window\]](#)

[\[in a new window\]](#)

[\[Download PPT slide\]](#)

Figure 5a: Transverse color-coded US image shows subcutaneous 4.5-mm nude mouse angiosarcoma tumor (arrows) after intravenous injection of MB_V (a) before and (b) 30 minutes after administration of anti-mouse VEGFR2 antibodies and (c) after injection of MB_C. Video intensity was substantially reduced after VEGFR2 blocking. Low video intensity was measured with MB_C before blocking with anti-mouse VEGF2 antibodies (c).



View larger version (168K):

[\[in this window\]](#)

[\[in a new window\]](#)

[\[Download PPT slide\]](#)

Figure 5b: Transverse color-coded US image shows subcutaneous 4.5-mm nude mouse angiosarcoma tumor (arrows) after intravenous injection of MB_V (a) before and (b) 30 minutes after administration of anti-mouse VEGFR2 antibodies and (c) after injection of MB_C. Video intensity was substantially reduced after VEGFR2 blocking. Low video intensity was measured with MB_C before blocking with anti-mouse VEGF2 antibodies (c).

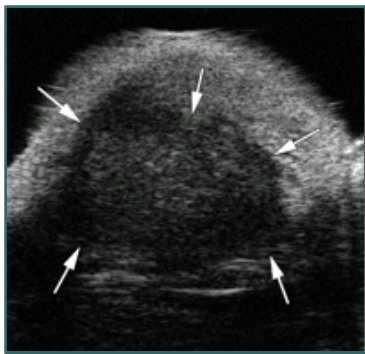


Figure 5c: Transverse color-coded US image shows subcutaneous 4.5-mm nude mouse angiosarcoma tumor (arrows) after intravenous injection of MB_v (a) before and (b) 30 minutes after administration of anti-mouse VEGFR2 antibodies and (c) after injection of MB_c. Video intensity was substantially reduced after VEGFR2 blocking. Low video intensity was measured with MB_c before blocking with anti-mouse VEGFR2 antibodies (c).

View larger version (164K):

[\[in this window\]](#)

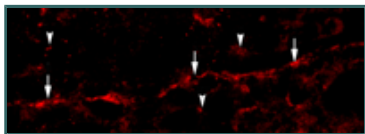
[\[in a new window\]](#)

[\[Download PPT slide\]](#)

Microbubble administration did not show any gross toxic effect, and all animals recovered after US imaging without any detectable signs of distress.

Tumor Immunohistochemical Results

Angiosarcoma and malignant glioma tumors stained positive for VEGFR2, which compared well with CD31-staining of vascular endothelial cells on adjacent tumor slices (Fig 6). This finding indicates expression of VEGFR2 on endothelial cells of tumor vessels.



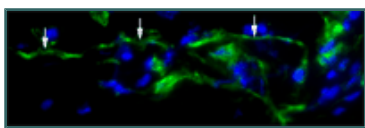
View larger version (34K):

[\[in this window\]](#)

[\[in a new window\]](#)

[\[Download PPT slide\]](#)

Figure 6a: Micrographs of adjacent frozen tissue slices of (a, b) angiosarcoma and (c, d) malignant glioma tumors after immunofluorescence staining of VEGFR2 (a and c) and CD31 (b and d). For VEGFR2 staining, slices were incubated with rat anti-mouse VEGFR2 primary antibody and Cy3-conjugated donkey anti-rat secondary antibody (red). For CD31 staining, slices were incubated with rat anti-mouse CD31 antibody and fluorescein isothiocyanate-conjugated donkey anti-rat secondary antibody (green); CD31-stained slices were counterstained with 4',6-diamidino-2-phenylindole (blue, cell nucleus). Both tumor types stained positive for VEGFR2 expression (a and c), referred to tumor vessels (arrows) on basis of adjacent CD31-stained tumor slices (b and d). Note slight additional VEGFR2 staining adjacent to tumor vessels in angiosarcoma tumors (arrowheads, a) resulting from SVR tumor cell staining. (Original magnification, x400.)



View larger version (35K):

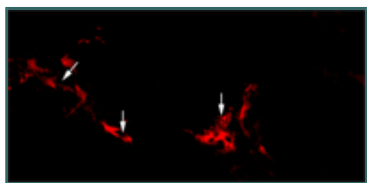
[\[in this window\]](#)

[\[in a new window\]](#)

[\[Download PPT slide\]](#)

Figure 6b: Micrographs of adjacent frozen tissue slices of (a, b) angiosarcoma and (c, d) malignant glioma tumors after immunofluorescence staining of VEGFR2 (a and c) and CD31 (b and d). For VEGFR2 staining, slices were incubated with rat anti-mouse VEGFR2 primary antibody and Cy3-conjugated donkey anti-rat secondary antibody (red). For CD31 staining, slices were incubated with rat anti-mouse CD31 antibody and fluorescein isothiocyanate-conjugated donkey anti-rat secondary antibody (green); CD31-stained slices were counterstained with

4',6-diamidino-2-phenylindole (blue, cell nucleus). Both tumor types stained positive for VEGFR2 expression (**a** and **c**), referred to tumor vessels (arrows) on basis of adjacent CD31-stained tumor slices (**b** and **d**). Note slight additional VEGFR2 staining adjacent to tumor vessels in angiosarcoma tumors (arrowheads, **a**) resulting from SVR tumor cell staining. (Original magnification, x400.)



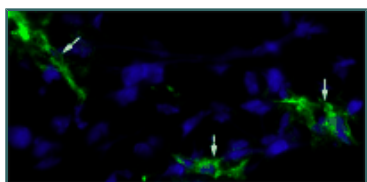
View larger version (14K):

[\[in this window\]](#)

[\[in a new window\]](#)

[\[Download PPT slide\]](#)

Figure 6c: Micrographs of adjacent frozen tissue slices of (**a**, **b**) angiosarcoma and (**c**, **d**) malignant glioma tumors after immunofluorescence staining of VEGFR2 (**a** and **c**) and CD31 (**b** and **d**). For VEGFR2 staining, slices were incubated with rat anti-mouse VEGFR2 primary antibody and Cy3-conjugated donkey anti-rat secondary antibody (red). For CD31 staining, slices were incubated with rat anti-mouse CD31 antibody and fluorescein isothiocyanate-conjugated donkey anti-rat secondary antibody (green); CD31-stained slices were counterstained with 4',6-diamidino-2-phenylindole (blue, cell nucleus). Both tumor types stained positive for VEGFR2 expression (**a** and **c**), referred to tumor vessels (arrows) on basis of adjacent CD31-stained tumor slices (**b** and **d**). Note slight additional VEGFR2 staining adjacent to tumor vessels in angiosarcoma tumors (arrowheads, **a**) resulting from SVR tumor cell staining. (Original magnification, x400.)



View larger version (45K):

[\[in this window\]](#)

[\[in a new window\]](#)

[\[Download PPT slide\]](#)

Figure 6d: Micrographs of adjacent frozen tissue slices of (**a**, **b**) angiosarcoma and (**c**, **d**) malignant glioma tumors after immunofluorescence staining of VEGFR2 (**a** and **c**) and CD31 (**b** and **d**). For VEGFR2 staining, slices were incubated with rat anti-mouse VEGFR2 primary antibody and Cy3-conjugated donkey anti-rat secondary antibody (red). For CD31 staining, slices were incubated with rat anti-mouse CD31 antibody and fluorescein isothiocyanate-conjugated donkey anti-rat secondary antibody (green); CD31-stained slices were counterstained with 4',6-diamidino-2-phenylindole (blue, cell nucleus). Both tumor types stained positive for VEGFR2 expression (**a** and **c**), referred to tumor vessels (arrows) on basis of adjacent CD31-stained tumor slices (**b** and **d**). Note slight additional VEGFR2 staining adjacent to tumor vessels in angiosarcoma tumors (arrowheads, **a**) resulting from SVR tumor cell staining. (Original magnification, x400.)

DISCUSSION

In this study, we demonstrated that in angiosarcoma and malignant glioma tumors, tumor angiogenesis can be assessed by using US imaging with contrast microbubbles labeled with monoclonal antibodies against murine VEGFR2. We first showed in the cell culture that MB_v preferentially adhered to murine SVR cells expressing VEGFR2. Binding of MB_v to negative control murine myoblast cells was greater than zero and substantially lower after blocking with anti-mouse VEGFR2 antibodies, which may indicate a degree of nonspecific adhesions of the

- ▲ [TOP](#)
- ▲ [ABSTRACT](#)
- ▲ [INTRODUCTION](#)
- ▲ [MATERIALS AND METHODS](#)
- ▲ [RESULTS](#)
- [DISCUSSION](#)
- ▼ [ADVANCE IN KNOWLEDGE](#)
- ▼ [IMPLICATION FOR PATIENT CARE](#)
- ▼ [References](#)

monoclonal antibodies to receptors other than VEGFR2. The magnitude of these adhesions, however, was minimal compared with the specific adhesive interactions of MB_V and there was almost no attachment of MB_N to both types of cells in cell culture. This suggests that neither the biotin moieties of the labeling antibodies nor the components of the microbubble shell, including lipids and streptavidin, contributed substantially to the adhesions.

We further tested the utility of antibody-labeled microbubbles in vivo to noninvasively and quantitatively imaged VEGFR2 expression in tumor vessels in two mouse tumor models. In both tumor models, there was little contrast enhancement after MB_C administration, possibly owing to nonspecific interactions of the isotype-matched control immunoglobulin G2 antibody with ligands of the vascular endothelium. This is consistent with our observation in cell culture that some MB_C also adhered to tumor cells. To further validate the specificity of MB_V binding to endothelial VEGFR2, we performed in vivo blocking studies which showed a substantial decrease of video intensity of anti-mouse VEGFR2 antibodies after intravenous administration.

To our knowledge, there is no animal tumor model without any form of angiogenesis, so we used normal hind limb skeletal muscle of the mice to show no persistent contrast enhancement of nonneoplastic/nonangiogenesis microvasculature after injection of MB_V. Strong VEGFR2 staining of tumor vessels in both tumor types with only slight and no staining of angiosarcoma and malignant glioma tumor cells, respectively, was confirmed with immunohistochemical analysis. This finding suggests that increased video signal after administration of MB_V was primarily caused by the attachment of microbubbles to tumor vessel endothelial cells of both tumor types and not by attachment of microbubbles to tumor cells. This supports the observation by Lindner (4) that microbubbles do not leak out of tumor vessels, owing to their size of several micrometers.

With the development of site-targeted probes, US contrast agents are evolving from pure blood pool contrast agents to molecular imaging agents designed for specific molecular targets present in the vascular compartment (4). Monoclonal antibodies that recognize endothelial cell adhesion molecules, such as P-selectin, intercellular adhesion molecule-1, and mucosal addressin cell adhesion molecule-1 have been conjugated to the surface of microbubbles for imaging of inflammation (15–17). Microbubbles targeted to the platelet glycoprotein IIb/IIIa integrin (18) and to fibrin (19) have been used for thrombus imaging.

Experience with imaging of angiogenesis with targeted contrast-enhanced US is still limited. Recently, targeted contrast-US applications have been extended for imaging angiogenesis in a rat model of ischemic hind limb skeletal muscle (20) and in a malignant tumor model in rats (5). By using biotinylated echistatin for labeling microbubbles, contrast-enhanced US imaging with microbubbles targeted to $\alpha_v\beta_3$ integrins have been shown to provide information on the spatial distribution and extent of tumor angiogenesis in malignant glioma tumors, including the detection of micrometastases (5).

Although the molecular target for the tumor-binding cyclic tripeptide arginine-arginine-leucine is as yet unknown, Weller et al (7) have shown proof-of-principle of US detection of angiogenic tumor vasculature in a tumor-bearing mouse model by using microbubbles conjugated to cyclic tripeptide arginine-arginine-leucine.

In our study, we demonstrated a proof of principle of targeted US angiogenesis imaging by using the critical endothelial marker of tumor angiogenesis VEGFR2 as a molecular imaging target. Since VEGF and/or VEGFR2 signaling is one of the most important pathways in tumor angiogenesis, the spatial visualization and quantitative assessment of VEGFR2 expression levels during tumor growth and at anticancer treatment may be of critical importance for various studies. For example, it has been shown that the therapeutic window of VEGF/VEGFR2-targeted delivery does not depend on the total dose

given but rather on the microenvironmental levels of VEGF/VEGFR2 expression (21). The visualization of VEGFR2 expression in vivo by using US imaging with contrast microbubbles targeted against VEGFR2 may help in optimization of current or novel anticancer treatment regimes by choosing the right timing during which the treatment is most effective.

Our study had limitations. First, cell attachment studies of microbubbles were not performed under flow conditions to simulate in vivo exposure of microbubbles to shear stress, which may influence the number of attached microbubbles to cells (22). In addition, microbubble attachment in cell culture may be directly compared with VEGFR2 densities in future studies by using cell lines with different defined receptor expression levels.

Second, the number of animals assessed in vivo was somewhat small. However, the highly significant differences between MB_V and MB_C did not justify the use of additional animals, according to the regulations of our Institutional Administrative Panel on Laboratory Animal Care.

Third, we did not directly correlate the magnitude of targeted US imaging signal levels with tumor vessel VEGFR2 expression levels, although we did blocking of molecular targets and control studies to validate our results. Furthermore, in tumor vessels not expressing VEGFR2, although unlikely, the described technique for monitoring tumor angiogenesis may be of limited value.

Finally, although prior studies have indicated that only a few retained microbubbles are required to produce a detectable signal (13,23), the overall sensitivity of VEGFR2-targeted US imaging for helping detect tumor angiogenesis with MB_V needs to be systematically studied. Additional studies that look at the effects of microbubble injected dose on imaging signal level, potential for toxicity and immunogenicity, other mouse models of angiogenesis, serial studies for monitoring antiangiogenesis and anti-VEGFR2 therapy, correlation of results with radionuclide-based strategies for imaging VEGFR2, and imaging of multiple molecular targets will all be useful for further implementation of targeted US imaging strategies and are currently under investigation.

In conclusion, the results of our study suggest that US imaging with contrast microbubbles allows noninvasive two-dimensional spatial visualization of VEGFR2 expression in tumor vessels in mice. This should have direct implications for future monitoring of antitumor and antiangiogenic therapies in neoplastic vasculature expressing VEGFR2 and for studying the biology of angiogenesis in living subjects.

Because contrast-enhanced US is already widely available in the medical community, clinical translation of targeted contrast-enhanced US imaging approaches in clinical application may be readily available, however, by using binding chemistry other than biotin-streptavidin. Postprocessing of targeted contrast-enhanced US imaging is made easy by using a computational algorithm that automatically color-codes the video intensity levels from adherent microbubbles on the gray-scale US images with a quantifiable measure of signal. In future practice, physicians could repeatedly obtain color-coded images of tumors, combined with a quantitative measure of signal, in a short period of time without causing any known health risk or particular discomfort to the patient.

▶ **ADVANCE IN KNOWLEDGE**

- Contrast-enhanced US imaging with microbubbles targeted to vascular endothelial growth factor receptor type 2 allows assessment of tumor angiogenesis in murine angiosarcoma and

▲ [TOP](#)
▲ [ABSTRACT](#)
▲ [INTRODUCTION](#)
▲ [MATERIALS AND METHODS](#)
▲ [RESULTS](#)

malignant glioma tumors.

- ▲ [DISCUSSION](#)
- [ADVANCE IN KNOWLEDGE](#)
- ▼ [IMPLICATION FOR PATIENT CARE](#)
- ▼ [References](#)

▶ **IMPLICATION FOR PATIENT CARE**

- Our work in small animals can provide groundwork information for eventual application of this US approach for molecular imaging of tumor angiogenesis in patients.

- ▲ [TOP](#)
- ▲ [ABSTRACT](#)
- ▲ [INTRODUCTION](#)
- ▲ [MATERIALS AND METHODS](#)
- ▲ [RESULTS](#)
- ▲ [DISCUSSION](#)
- ▲ [ADVANCE IN KNOWLEDGE](#)
- [IMPLICATION FOR PATIENT CARE](#)
- ▼ [References](#)

▶ **ACKNOWLEDGMENTS**

The authors thank Jarrett Rosenberg, PhD, Department of Radiology, Stanford University, San Francisco, Calif, for assistance with statistical analysis.

▶ **FOOTNOTES**

Abbreviations: MB_C = control microbubble • MB_N = nontargeted microbubble • MB_V = VEGF R2–targeted microbubble • PBS = phosphate-buffered saline • VEGF = vascular endothelial growth factor • VEGFR2 = VEGF receptor 2 • VI_T = mean video intensity difference

Guarantors of integrity of entire study, J.K.W., S.S.G.; study concepts/study design or data acquisition or data analysis/interpretation, all authors; manuscript drafting or manuscript revision for important intellectual content, all authors; final manuscript version approved, all authors; literature research, J.K.W.; experimental studies, J.K.W., R.P., K.C.; statistical analysis, J.K.W.; and manuscript editing, J.K.W., R.P., S.S.G.

▶ **References**

1. Kerbel R, Folkman J. Clinical translation of angiogenesis inhibitors. *Nat Rev Cancer* 2002;2:727–739. [[Medline](#)]
2. Hicklin DJ, Ellis LM. Role of the vascular endothelial growth factor pathway in tumor growth and angiogenesis. *J Clin Oncol* 2005;23:1011–1027. [[Abstract/Free Full Text](#)]
3. Folkman J. Angiogenesis. *Annu Rev Med* 2006;57:1–18. [[Medline](#)]
4. Lindner JR. Microbubbles in medical imaging: current applications and future directions. *Nat Rev Drug Discov* 2004;3:527–532. [[Medline](#)]
5. Ellegala DB, Leong-Poi H, Carpenter JE, et al. Imaging tumor angiogenesis with contrast ultrasound and microbubbles targeted to alpha(v) beta3. *Circulation* 2003;108:336–341. [[Medline](#)]
6. Korpanty G, Carbon JG, Grayburn PA, Fleming JB, Brekken RA. Monitoring response to anticancer therapy by targeting microbubbles to tumor vasculature. *Clin Cancer Res* 2007;13:323–330. [[Abstract/Free Full Text](#)]
7. Weller GE, Wong MK, Modzelewski RA, et al. Ultrasonic imaging of tumor angiogenesis using contrast microbubbles targeted via the tumor-binding peptide arginine-arginine-leucine. *Cancer Res*

- ▲ [TOP](#)
- ▲ [ABSTRACT](#)
- ▲ [INTRODUCTION](#)
- ▲ [MATERIALS AND METHODS](#)
- ▲ [RESULTS](#)
- ▲ [DISCUSSION](#)
- ▲ [ADVANCE IN KNOWLEDGE](#)
- ▲ [IMPLICATION FOR PATIENT CARE](#)
- [References](#)

- 2005;65:533–539. [[Abstract/Free Full Text](#)]
8. Villanueva FS, Jankowski RJ, Klivanov S, et al. Microbubbles targeted to intercellular adhesion molecule-1 bind to activated coronary artery endothelial cells. *Circulation* 1998;98:1–5. [[Medline](#)]
 9. Grobden B, De Deyn PP, Slegers H. Rat C6 glioma as experimental model system for the study of glioblastoma growth and invasion. *Cell Tissue Res* 2002;310:257–270. [[Medline](#)]
 10. Arrieta O, Guevara P, Reyes S, Ortiz A, Rembao D, Sotelo J. Protamine inhibits angiogenesis and growth of C6 rat glioma: a synergistic effect when combined with carmustine. *Eur J Cancer* 1998;34:2101–2106. [[Medline](#)]
 11. Bai X, Cerimele F, Ushio-Fukai M, et al. Honokiol, a small molecular weight natural product, inhibits angiogenesis in vitro and tumor growth in vivo. *J Biol Chem* 2003;278:35501–35507. [[Abstract/Free Full Text](#)]
 12. Arbiser JL, Moses MA, Fernandez CA, et al. Oncogenic H-ras stimulates tumor angiogenesis by two distinct pathways. *Proc Natl Acad Sci U S A* 1997;94:861–866. [[Abstract/Free Full Text](#)]
 13. Lindner JR, Song J, Xu F, et al. Noninvasive ultrasound imaging of inflammation using microbubbles targeted to activated leukocytes. *Circulation* 2000;102:2745–2750. [[Abstract/Free Full Text](#)]
 14. Wei K, Jayaweera AR, Firoozan S, Linka A, Skyba DM, Kaul S. Quantification of myocardial blood flow with ultrasound-induced destruction of microbubbles administered as a constant venous infusion. *Circulation* 1998;97:473–483. [[Medline](#)]
 15. Bachmann C, Klivanov AL, Olson TS, et al. Targeting mucosal addressin cellular adhesion molecule (MAdCAM)-1 to noninvasively image experimental Crohn's disease. *Gastroenterology* 2006;130:8–16. [[Medline](#)]
 16. Lindner JR, Song J, Christiansen J, Klivanov AL, Xu F, Ley K. Ultrasound assessment of inflammation and renal tissue injury with microbubbles targeted to P-selectin. *Circulation* 2001;104:2107–2112. [[Abstract/Free Full Text](#)]
 17. Weller GE, Lu E, Csikari MM, et al. Ultrasound imaging of acute cardiac transplant rejection with microbubbles targeted to intercellular adhesion molecule-1. *Circulation* 2003;108:218–224. [[Medline](#)]
 18. Unger EC, McCreery TP, Sweitzer RH, Shen D, Wu G. In vitro studies of a new thrombus-specific ultrasound contrast agent. *Am J Cardiol* 1998;81:58G–61G. [[Medline](#)]
 19. Lanza GM, Wallace KD, Scott MJ, et al. A novel site-targeted ultrasonic contrast agent with broad biomedical application. *Circulation* 1996;94:3334–3340. [[Medline](#)]
 20. Leong-Poi H, Christiansen J, Heppner P, et al. Assessment of endogenous and therapeutic arteriogenesis by contrast ultrasound molecular imaging of integrin expression. *Circulation* 2005;111:3248–3254. [[Abstract/Free Full Text](#)]
 21. Cai W, Rao J, Gambhir SS, Chen X. How molecular imaging is speeding up antiangiogenic drug development. *Mol Cancer Ther* 2006;5:2624–2633. [[Abstract/Free Full Text](#)]
 22. Weller GE, Villanueva FS, Klivanov AL, Wagner WR. Modulating targeted adhesion of an ultrasound contrast agent to dysfunctional endothelium. *Ann Biomed Eng* 2002;30:1012–1019. [[Medline](#)]
 23. Klivanov AL, Rasche PT, Hughes MS, et al. Detection of individual microbubbles of ultrasound contrast agents: imaging of free-floating and targeted bubbles. *Invest Radiol* 2004;39:187–195. [[Medline](#)]

This Article

- ▶ [Abstract](#) **FREE**
- ▶ [Figures Only](#)
- ▶ [Appendix E1](#)
- ▶ [Submit a response](#)
- ▶ [Alert me when this article is cited](#)
- ▶ [Alert me when eLetters are posted](#)
- ▶ [Alert me if a correction is posted](#)
- ▶ [Citation Map](#)

Services

- ▶ [Email this article to a friend](#)
- ▶ [Similar articles in this journal](#)

- ▶ [Similar articles in PubMed](#)
- ▶ [Alert me to new issues of the journal](#)
- ▶ [Download to citation manager](#)
- ▶ [© Get Permissions](#)

Google Scholar

- ▶ [Articles by Willmann, J. K.](#)
- ▶ [Articles by Gambhir, S. S.](#)

PubMed

- ▶ [PubMed Citation](#)
- ▶ [Articles by Willmann, J. K.](#)
- ▶ [Articles by Gambhir, S. S.](#)

HOME HELP FEEDBACK SUBSCRIPTIONS ARCHIVE SEARCH
RADIOLOGY RADIOGRAPHICS RSNA JOURNALS ONLINE